Is There a Role for Human-Induced Climate Change in the Precipitation Decline that Drove the California Drought?

RICHARD SEAGER, NAOMI HENDERSON, MARK A. CANE, HAIBO LIU, AND JENNIFER NAKAMURA

Lamont-Doherty Earth Observatory, Columbia University, Palisades, New York

(Manuscript received 24 March 2017, in final form 21 August 2017)

ABSTRACT

The recent California drought was associated with a persistent ridge at the west coast of North America that has been associated with, in part, forcing from warm SST anomalies in the tropical west Pacific. Here it is considered whether there is a role for human-induced climate change in favoring such a west coast ridge. The models from phase 5 of the Coupled Model Intercomparison Project do not support such a case either in terms of a shift in the mean circulation or in variance that would favor increased intensity or frequency of ridges. The models also do not support shifts toward a drier mean climate or more frequent or intense dry winters or to tropical SST states that would favor west coast ridges. However, reanalyses do show that over the last century there has been a trend toward circulation anomalies over the Pacific–North American domain akin to those during the height of the California drought. The trend has been associated with a trend toward preferential warming of the Indo–west Pacific, an arrangement of tropical oceans and Pacific–North American circulation similar to that during winter 2013/14, the driest winter of the California drought. These height trends, however, are not reproduced in SST-forced atmosphere model ensembles. In contrast, idealized atmosphere modeling suggests that increased tropical Indo-Pacific zonal SST gradients are optimal for forcing height trends that favor a west coast ridge. These results allow a tenuous case for human-driven climate change driving increased gradients and favoring the west coast ridge, but observational data are not sufficiently accurate to confirm or reject this case.

1. Introduction

The California drought entered its sixth year in fall 2016 having survived the 2015/16 massive El Niño winter. During summer 2016 California experienced a record fire season, and drought impacts across the state on agriculture, rural and city water supplies, and ecosystems have been profound. Human-driven climate change has become a part of our daily reality. July 2016 was the hottest month on record for global average temperature (http://www.noaa.gov/news/july-was-hottest-month-on-record-for-globe, accessed 14 August 2017), globally 2016 was the warmest year on record (https://www.nasa.gov/press-release/nasa-noaa-data-show-2016-warmest-year-on-record-globally, accessed 14 August 2017), and records for warmest global and annual mean temperature have been set five times in the twenty-first century (https://www.ncdc.noaa.gov/sotc/global/201613, accessed 14 August 2017). For individual weather and climate events it is generally easier to detect a human contribution to warm extremes than it is for precipitation extremes [see reviews by Shepherd (2015) and Stott et al. (2016)], although cases have been made for greenhouse gas (GHG)-driven drying trends making the severity and persistence of recent droughts more likely [e.g., Kelley et al. (2015) for the case of the Middle East]. It is often suggested, or asserted, that the California drought has an anthropogenic component. For example, Wang et al. (2014) and Swain et al. (2014) both claim that the persistence and amplitude of the west coast ridge was partly attributable to forcing from rising GHGs. In contrast, Seager et al. (2014a, 2015), Seager and Henderson (2016), Hartmann (2015), Lee et al. (2015), Watson et al. (2016), and Teng and Branstator (2017) emphasize natural variability and the role of SST and tropical precipitation anomalies in driving the ridge. These papers all invoke, to greater or lesser extent, warm SST anomalies in the western tropical Pacific Ocean and,

Corresponding author: Richard Seager, seager@ldeo.columbia.edu

DOI: 10.1175/JCLI-D-17-0192.1

variously, additional warm anomalies in the Indian Ocean and cool anomalies in the central equatorial Pacific as was characteristic of winter 2013/14 and early 2015 when drought over California persisted. In contrast to the precipitation reduction, there is little serious doubt that warm temperature anomalies contributed to the drought by driving down surface moisture conditions and that rising GHGs contributed to the warming (Williams et al. 2015).

In this paper we consider whether a case may be made for a human role in the precipitation loss that is the prime driver of the California drought. At face value this seems unlikely. Neelin et al. (2013) and Seager et al. (2015) both point out that the models participating in phase 5 of the Coupled Model Intercomparison Project (CMIP5) and assessed by the Intergovernmental Panel on Climate Change Fifth Assessment Report show a modest increase in winter precipitation in central and northern California as a consequence of rising GHGs. However, Simpson et al. (2016) have argued that the amplitude of this wet trend is overestimated owing to CMIP5 model bias in the simulation and response to rising GHGs of intermediate-scale planetary waves. They show, nonetheless, that the subset of models that best simulate the relevant wave field still project an increase in winter precipitation for California, albeit one that is smaller than the multimodel mean. Despite these results we can think of a number of ways in which the precipitation drop might be related to human-induced climate change:

- Though the mean change for California is a wetting, the variability changes such that dry winters become more likely and/or more severe.
- West coast ridges during winter are becoming more likely as a consequence of an atmospheric or atmosphere–ocean response to rising GHGs. Since the multimodel mean of CMIP5 projections is toward a trough west of North America (Neelin et al. 2013; Seager et al. 2014b; Simpson et al. 2016), this could be a consequence of a change in circulation variability or perhaps model projections are simply wrong.
- Even though CMIP5 models tend to have more GHG-driven warming in the eastern equatorial Pacific than in the west (Li et al. 2016), changes in tropical Pacific variability will make winters with an increased east–west SST gradient akin to winter 2013/14 more likely driving an atmospheric response with a west coast ridge.
- Reductions in Arctic sea ice alter the extratropical Northern Hemisphere circulation in a way that favors a west coast ridge. CMIP5 models do simulate sea ice loss but may be missing or understating California-drying–Arctic sea ice loss teleconnections.
- As a group, the CMIP5 models are wrong and the tropical Indo-Pacific climate system is responding to rising GHGs by strengthening west–east SST gradients (Clement et al. 1996; Cane et al. 1997; Kohyama et al. 2017; Kohyama and Hartmann 2017), making SST anomaly patterns like that of winter 2013/14 more likely.

We will examine each of these possibilities using CMIP5 models, atmosphere models forced with historical SSTs, observation-based reanalyses, and idealized modeling. It will be shown that it is hard to make a case based on the CMIP5 models that human-driven climate change contributed to the precipitation loss during the California drought. Instead we will conclude by building a case for what needs to have occurred in the real climate system in order for the loss of precipitation during the CA drought to have a contribution from changes in radiative forcing. This case relies on positive radiative forcing causing increasing zonal asymmetry of tropical SSTs, and, while we think this is plausible and consistent with the observational record to date, the response is contrary to that in CMIP5 climate models. Hence, acceptance of this argument requires a bold rejection of modeling consensus. At this point, a combination of structural model bias and the limitations of the observational record preclude a firm conclusion as to the causes of this example of climate change in regions where the tropics exert an important influence.

2. Observational data and model simulations

For the observational and model analyses all results are for the six-month winter half-year average from November through April, which reflects the persistence of the west coast ridge through the winters of the California drought. Anomalies are relative to a winter 1979/80 to 2013/14 average.

a. Observations

For observations we make use of multiple atmospheric reanalyses that cover a sufficiently long time period to study decadal time scale trends. We use the European Centre for Medium-Range Weather Forecasts (ECMWF) interim reanalysis (ERA-Interim; Dee et al. 2011) from 1979 to 2015 and extend back to 1958 by concatenating with ERA-40 (Uppala et al. 2005). We also use the National Centers for Environmental Prediction–National Center for Atmospheric Research (NCEP–NCAR) reanalysis (Kalnay et al. 1996; Kistler et al. 2001) from 1958 to 2015. Finally we use the NCEP Twentieth Century Reanalysis (20CR; Compo et al. 2011)

from 1900 to 2014. Of these, ERA40/ERA-Interim and NCEP–NCAR assimilate all available data, but the 20CR assimilates only surface pressure data. We also use the SST datasets provided by these reanalyses and which directly impact the atmospheric state in the reanalyses. In addition we use the precipitation. We know well enough to not have too much faith in the reanalysis precipitation estimates, but over the oceans, for the long periods we need to consider, they are the only data available. Our purpose in examining the precipitation is merely to look at the connection between SST and precipitation trends within the tropical Indo-Pacific region on a large scale, and we do consider the reanalysis precipitation potentially adequate for that purpose. We also analyze monthly sea ice anomalies as taken from the National Oceanic and Atmospheric Administration (NOAA) National Sea Ice Data Center (NSIDC) data based on remote sensing and covering 1979 to 2015 (http://nsidc.org/data/g02202).

b. *Model simulations*

We make use of three different kinds of model simulations.

1) CMIP5 COUPLED MODEL SIMULATIONS OF THE HISTORICAL PERIOD AND PROJECTIONS OF THE FUTURE

We make use of all available runs with all available models that supply the data we needed from CMIP5. This was 38 models (Table 1). We analyzed the historical period of 1979 to 2005 and the future projections using the RCP85 emissions scenario. The models were regridded to a common $2° \times 2°$ grid.

2) SST-FORCED SIMULATIONS WITH ATMOSPHERE MODELS

We use the seven models analyzed in association with the NOAA Drought Task Force (DTF) by Seager et al. (2014a, 2015). These variously extend from the nineteenth century, 1958, or 1979 to present and have ensembles varying from 10 to 57 members. The models are the NCAR Community Climate Model, version 3 (CCM3); two versions of the NOAA Climate Forecast System version 2 atmosphere model—one run by the Climate Prediction Center (CPC; CFSv2) and one by the Earth System Research Laboratory (ESRL-GFSv2); the NCAR Community Atmosphere Model, version 4 (CAM4); the ECMWF–Max Planck Institute–Hamburg models, versions 4.5 and 5 (ECHAM4.5 and ECHAM5); and the National Aeronautics and Space Administration (NASA) Goddard Earth Observing System, version 5 (GEOS-5). In addition we analyze a 16-member NCAR CAM5 ensemble recently completed at Lamont.

3) IDEALIZED "AREA SST" SIMULATIONS

To address trends in circulation over the North Pacific–North America sector we make use of 100-member ensemble simulations forced by imposed SSTs in various areas. This is akin to the "box SST" experiments Seager and Henderson (2016) used to analyze the particular case of winter 2013/14. The SST trends over past decades in the Indian and west Pacific Oceans are much more spatially broad than the SST anomalies in 2013/14, so here we use imposed SST anomalies over larger areas than used before. The exception is the cold tongue region of the equatorial Pacific where we impose an equatorially confined anomaly. The five areas are the Indian Ocean [35°S–35°N, 30°–120°E], Maritime Continent [25°S–25°N, 80°–160°E], west Pacific [25°S – 25°N, 120°E – 170°W], cold tongue 5°S – 5°N, 170°W to the South American coast, and a final one in which a uniform increase of SST is imposed over all ice-free ocean areas 60°S – 60°N. For each area, +1° and −1°C anomalies are imposed after two passes of a 1–2–1 smoother to remove the sharp transition at the edges of the areas, and a 100-member ensemble is generated for each. This creates 10 ensemble mean responses that are used in the optimization analysis described below.

3. Results

a. *Possibility 1: The CMIP5 models are right—Changes in the CMIP5 ensemble of atmosphere–ocean states of relevance to California drought*

1) CHANGES IN MEAN AND VARIANCE OF PRECIPITATION

To assess the change in precipitation P, we used the 38 CMIP5 models and identified those grid boxes that overlap with California. Within each model and ensemble member anomalies are computed relative to a 1979–2005 climatology within the models' historical runs. Anomalies are computed for the historical period, the current decade (2011–20) and the next two decades (2021–40). Rather unconventionally we present the results for the differences relative to the 1979–2005 climatology of the individual winters of the individual ensemble members. Hence, for each time period the sample is the $N = N_{\text{years}} \times \sum_{m=1}^{M} N_{m,\text{ens}}$, where N_{years} is the number of years (10 for 2011–20 and 20 for 2021–40), $N_{m,\text{ens}}$ is the number of ensemble members for model m, and M is the total number of models. This provides a grand distribution of anomalies that we further divide into upper, upper middle, lower middle, and lower quartiles.

TABLE 1. CMIP5 models used in this study, their ensemble size, institution, and horizontal and vertical resolution.

Model	Ensemble size	Institute	Resolution (lon × lat), level
1. ACCESS1.0	1	Commonwealth Scientific and Industrial Research Organization	N96 (1.25° × 1.875°), L38
2. ACCESS1.3	1	(CSIRO), and Bureau of Meteorology, Australia (BoM)	N96 (1.25° × 1.875°), L38
3. BCC_CSM1.1	1	Beijing Climate Center, China Meteorological Administration	T42 (2.81° × 2.77°), L26
4. BCC_CSM1.1(m)	1		T106, L26
5. BNU-ESM	1	College of Global Change and Earth System Science, Beijing Normal University (BNU)	T42, L26
6. CanESM2	5	Canadian Centre for Climate Modelling and Analysis (CCCma)	T63 (1.875° × 1.875°), L35
7. CCSM4	6	NCAR	1.25° × 0.9°, L26
8. CESM1(BGC)	1	Community Earth System Model contributors (NSF–DOE–NCAR)	1.25° × 0.94°, L60
9. CESM1(CAM5)	3		1.25° × 0.94°, L30
10. CMCC-CESM*	1	Centro Euro-Mediterraneo per I Cambiamenti Climatici (CMCC)	T31, L39
11. CMCC-CM	1		T159, L31
12. CMCC-CMS	1		T63, L95
13. CNRM-CM5	5	Centre National de Recherches Météorologiques–Centre Européen de Recherche et de Formation Avancée en Calcul Scientifique (CNRM–CERFACS)	T127 (1.4° × 1.4°), L31
14. CSIRO Mk3.6.0	10	CSIRO in collaboration with the Queensland Climate Change Centre of Excellence (CSIRO–QCCCE)	T63 (1.875° × 1.875°), L18
15. FGOALS-g2	1	Institute of Atmospheric Physics, Chinese Academy of Sciences and Tsinghua University (LASG-CESS)	128 × 60, L26
16. FIO-ESM	3	The First Institute of Oceanography, State Oceanic Administration	T42, L26
17. GFDL CM3	1	NOAA/Geophysical Fluid Dynamics Laboratory	C48 (2.5° × 2.0°), L48
18. GFDL-ESM2G	1	(NOAA/GFDL)	2.5° × 2.0°, L24
19. GFDL-ESM2M	1		2.5° × 2.0°, L24
20. GISS-E2-H	2	NASA Goddard Institute for Space Studies (NASA GISS)	2.5° × 2.0°, L40
21. GISS-E2-H-CC	1		2.5° × 2.0°, L40
22. GISS-E2-R	2		2.5° × 2.0°, L40
23. GISS-E2-R-CC	1		2.5° × 2.0°, L40
24. HadGEM2-CC**	1	Met Office Hadley Centre	N96, L38
25. HadGEM2-ES**	4		N96, L38
26. INM-CM4.0	1	Institute for Numerical Mathematics (INM)	2.0° × 1.5° L21
27. IPSL-CM5A-LR	4	L'Institut Pierre-Simon Laplace (IPSL)	3.75° × 1.875°, L39
28. IPSL-CM5A-MR	1		2.5° × 1.25°, L39
29. IPSL-CM5B-LR	1		3.75° × 1.875°, L39
30. MIROC5	3	Atmosphere and Ocean Research Institute (AORI; the	T85, L40
31. MIROC-ESM	1	University of Tokyo), National Institute for Environmental	T42, L80
32. MIROC-ESM-CHEM	1	Studies (NIES), and Japan Agency for Marine-Earth Science and Technology (JAMSTEC)	T42, L80
33. MPI-ESM-LR	3	Max Planck Institute for Meteorology (MPI-M)	T63, L47
34. MPI-ESM-MR	1		T63, L95
35. MRI-CGCM3	1	Meteorological Research Institute (MRI)	TL159 (1.125° × 1.125°), L48
36. MRI-ESM1	1		TL159 (1.125° × 1.125°), L48
37. NorESM1-M	1	Norwegian Climate Centre (NCC)	2.5° × 1.875°, L26
38. NorESM1-ME	1		2.5° × 1.875°, L26

The analysis done this way examines whether the statistical distribution of winter climate states alters as a consequence of changes in radiative forcing in the model worlds. In particular, do extreme dry winters become more common or is there a shift toward drier winters? Indeed, simple thermodynamic concepts of rising specific humidity following warming air temperatures lead to expectation that interannual hydroclimate variability will increase unless other dynamical factors interfere (Seager et al. 2012). Results are presented in Fig. 1 in terms of maps of the average across the upper and lower and two middle quartiles and box-and-whisker diagrams of the grand distribution. The box and whiskers show no evidence of either wet or dry extremes in P becoming more common or more extreme, and the changes in the mean and median of winter values are also very small. The quartile maps for 2021–40 confirm these conclusions. Over California the driest (wettest) quarter of winters is no drier (wetter) than during 1979–2005. This is consistent with Berg and Hall (2015), who show little

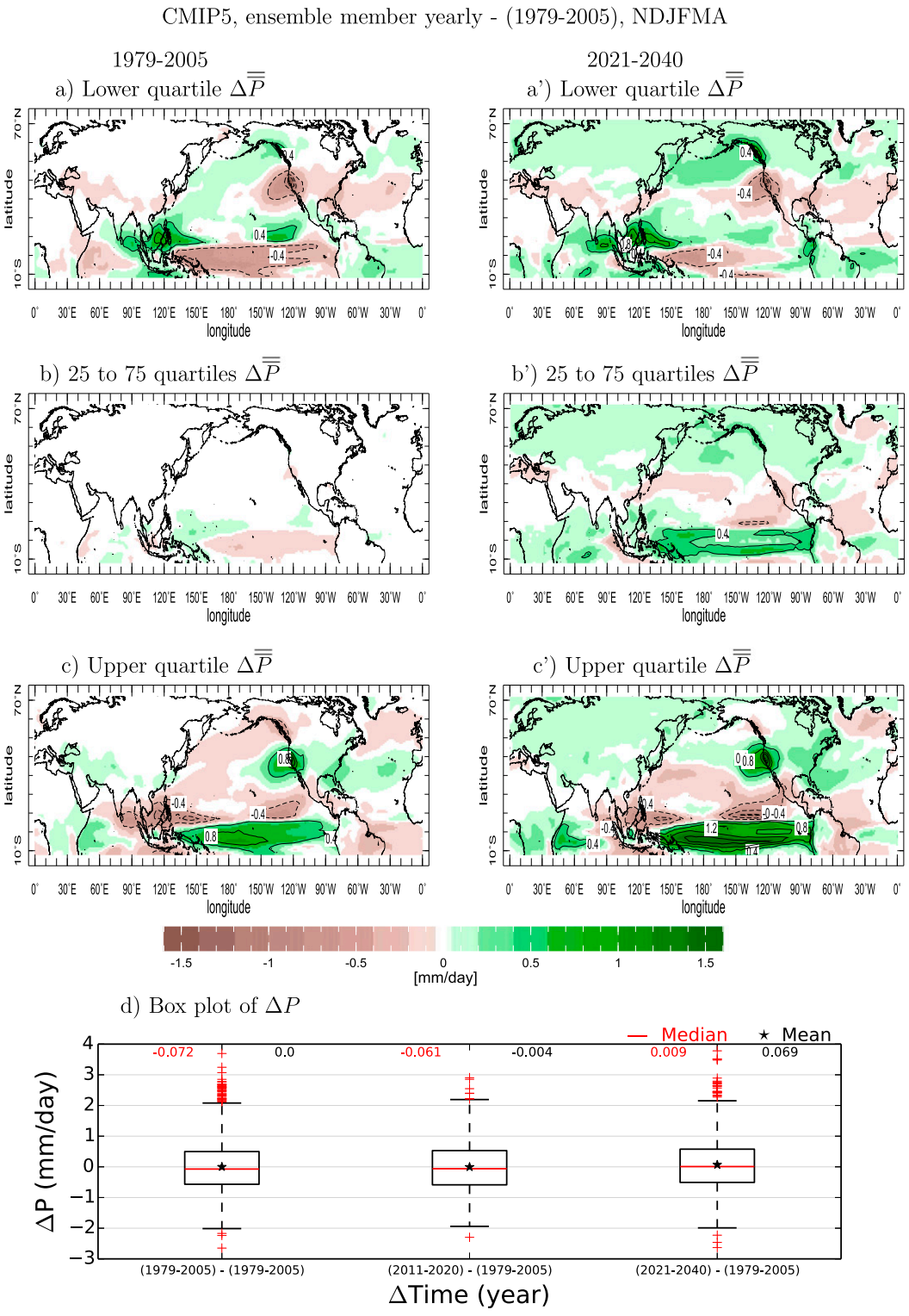

FIG. 1. Results for the grand distribution across all winters and all ensemble members and all models for *P*. Anomalies are relative to the model climatological means for 1979–2005. Maps show averages across the lower, two middle, and upper quartiles of the distributions for (left) 1979–2005 and (right) 2021–40. The box-and-whisker plots show the full distributions for 1979–2005, the current decade 2011–20, and the next two decades 2021–40. Units are mm day^{-1}.

change in frequency of dry winters for California in the coming decades (but do show increasing frequency of wet winters later in the century). The analysis was repeated for precipitation minus evapotranspiration, $P - E$, which accounts for the loss of water back to the atmosphere and which sustains runoff and change in soil moisture, and the results, which are not shown here, lead to the same conclusion of no change toward increased or more frequent dry extremes.

2) Changes in mean and variance of geopotential heights at the North American west coast

While we find no CMIP5 model-based evidence of increasing drought risk in California, it is possible that rising GHGs make ridges at the west coast more likely and/or stronger and that the models are missing the connection of this to P and $P - E$. To examine this we have computed the value of the 200-mb height field in a region spanned by 20°−60°N and 150°−120°W, which encompasses the region of high heights during the 2013/14 driest winter of the California drought. A simple result of global warming is that the atmosphere warms and expands raising geopotential heights. However, winds are related by geostrophy to gradients of height fields. Hence, we do this analysis on the fields with the zonal mean removed (eddy geopotential height $\langle\phi\rangle$), which gets more directly at the changes that are related to changes in circulation. Again we analyze the distribution across all winters, ensemble members, and models to assess whether the models indicate that extreme highs at the west coast become more likely even if the mean is toward lower heights.

Results are shown in Fig. 2. For the historical period the maps of the upper and lower quartiles show circulation anomalies that are essentially equal and opposite of each other with ridges and troughs at the west coast of North America contained within a wave train seemingly originating from the tropical Pacific Ocean. The wave train is likely ENSO forced, but we did not examine the association to SST anomalies. For the future two-decade period the maps show essentially the same wave features but now the troughs in the lower quartile are deeper and the ridges in the upper quartile less high. Notably the middle two quartiles have shifted to a weak trough at the west coast. The changes in the statistical distribution of individual winter circulation anomalies, presented in the maps and box-and-whisker plots, are consistent with a shift in the mean state toward a trough at the west coast and over the western North Pacific as in Neelin et al. (2013), Seager et al. (2014b, 2015), and Simpson et al. (2016) while retaining the same variance of height anomalies about the mean. Thus, according to the CMIP5 models, extreme west coast ridges become weaker as a consequence of climate change. The physical reasons for this detail of extratropical northern winter circulation change are not fully understood (Simpson et al. 2014), and it has been argued that the shift toward lower heights is likely overestimated (Simpson et al. 2016).

3) Changes in mean and variance of tropical Pacific SSTs

The above results notwithstanding, it is possible that the CMIP5 models create changes in the ocean states that should induce west coast ridges and droughts in California but miss the atmospheric teleconnection. As mentioned in the introduction, several papers have argued that warm SST anomalies in the tropical west Pacific Ocean and an increased west–east SST gradient across the tropical Pacific (Seager et al. 2015; Seager and Henderson 2016) contributed modestly but importantly to creating drought in winters 2011/12 to 2013/14. Hence, we examined changes in the CMIP5 models of west (15°S − 15°N, 130°E − 160°W) and east (10°S − 10°N, 140°−80°W) tropical Pacific SSTs and their difference again using the grand distribution across all winters in all ensemble members and all models. Results are presented in Fig. 3 in the same ways as for changes in P and $\langle\phi\rangle$. For the historical period the compositing on the west–east SST gradient shows in the maps the different phases of the model El Niño–Southern Oscillation (ENSO) cycles in the lower and upper quartiles. For the future period this is also the case but now amid a generally warming mean state of the oceans. Any change in the west–east SST gradient is more easily detected in the box-and-whisker plots where positive values indicate an increased gradient, which is more favorable for a west coast ridge and drought. The models do predict a steady but modest decrease from historical to current to future periods in the extreme high SST gradient winters. The models also project similarly modest decreases in the mean and median SST gradient and a 25th-percentile SST gradient that weakens. The CMIP5 models do not project an increase in the likelihood or strength of the SST state that has been invoked to partially explain the west coast ridge and drought.

b. Possibility 2: The CMIP5 models are wrong—Observed changes in atmosphere–ocean states of relevance to California drought and the case of Arctic sea ice

While we have little choice but to use models to project the future we should never be blind to the possibility that our models are wrong. Here we use observations to examine how the incidence of west coast

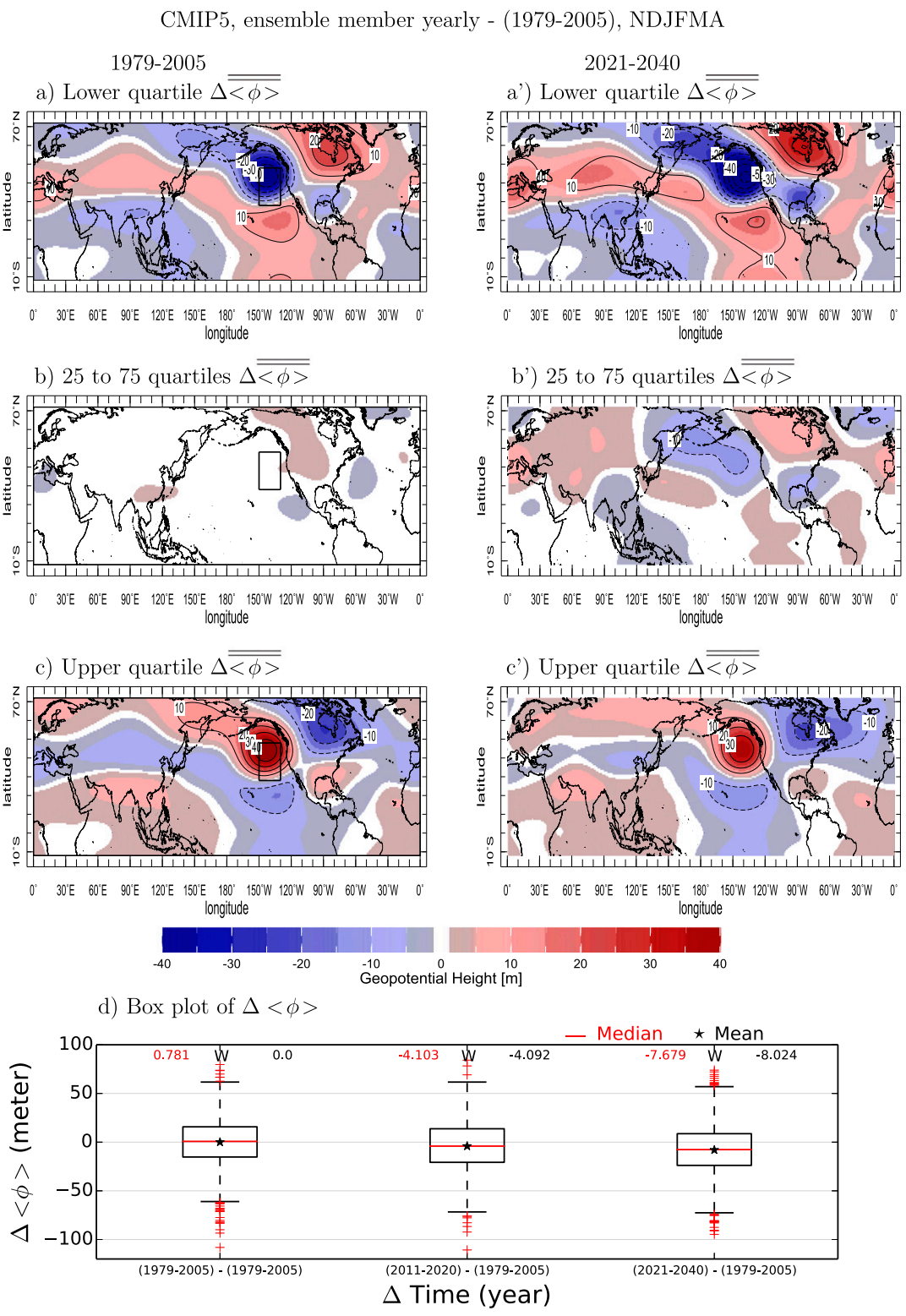

FIG. 2. As in Fig. 1, but for the departure of 200-mb geopotential height from its zonal mean $\langle\phi\rangle$. (b) The box for the height evaluation is shown. Units are meters.

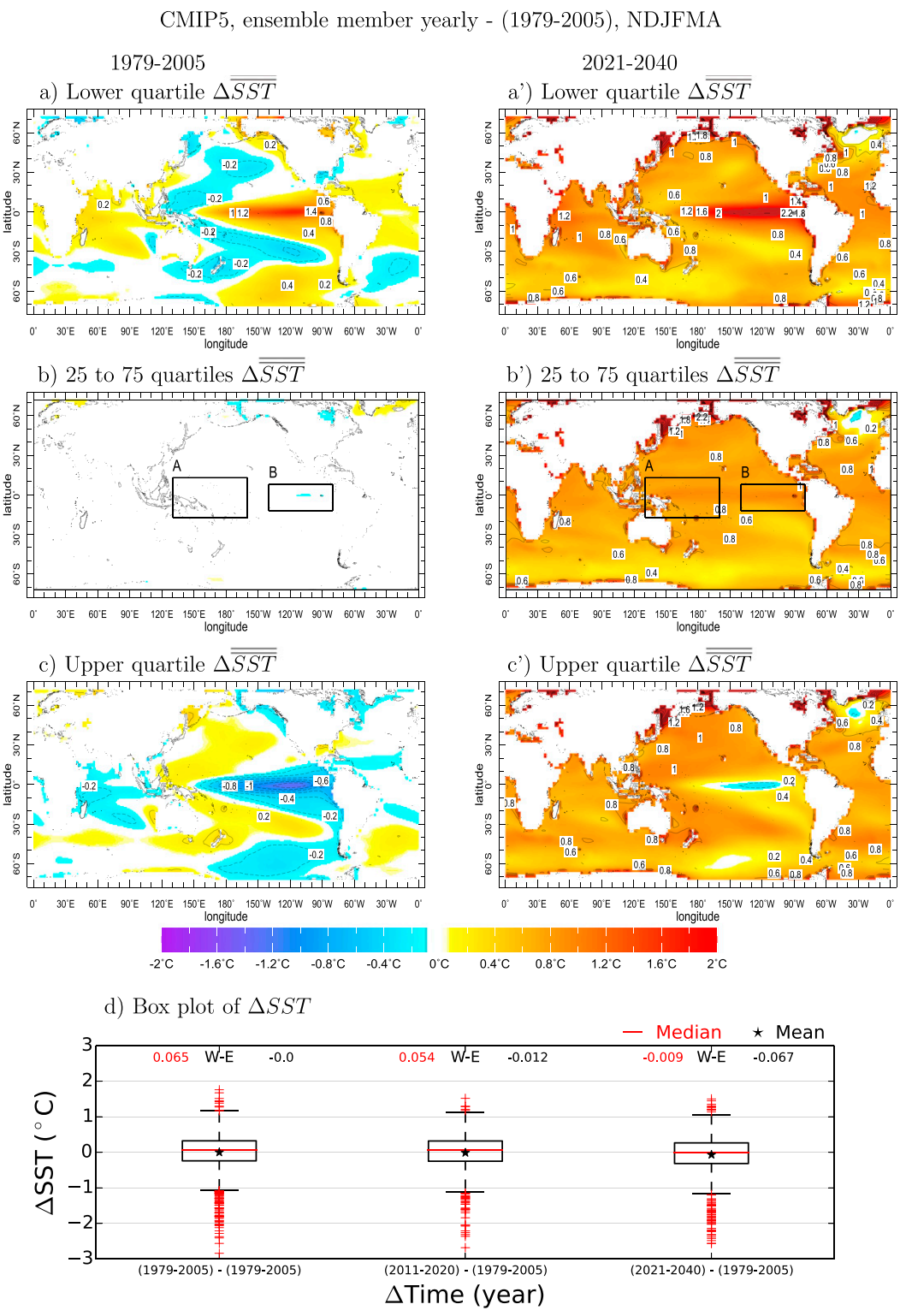

FIG. 3. As in Fig. 1, but for SST. (b) Western (box A) and eastern (box B) tropical Pacific boxes where the SSTs are computed are shown. Units are K.

ridges has changed and whether there is evidence for a link between sea ice variations and California precipitation.

1) HAS THE DROUGHT-INDUCING WEST COAST RIDGE BECOME MORE COMMON AND, IF SO, WHY?

To examine this we compute the spatial pattern correlation between the observed 200mb geopotential height anomaly for November 2013 to April 2014 and previous winters and plot time series of the pattern correlation coefficient. The area over which the pattern correlation is performed corresponds to the Pacific–North American region of interest and is 20°−80°N, 120°E − 40°W. This was first done for the NCEP–NCAR, ERA-40/ERA-Interim, and 20CR atmospheric reanalyses and is shown in Fig. 4. The November 2013 to April 2014 200-mb height and SST anomalies for the three reanalyses are also shown as maps. For their overlapping periods results from the three reanalyses agree well. Earlier winters have had similar events (notably winter 1993/94), but there is no really good analog to winter 2013/14. For the nearly seven-decade period covered by NCEP–NCAR there is no clear trend toward height patterns more akin to that which occurred in winter 2013/14. However the longer 20CR does show that such events were very unlikely in the first half of the twentieth century. Although the positive trend in 20CR is significant at the 95% level, we do not place too much confidence in this result alone given the declining data density in those distant decades.

Next we perform a similar analysis with the ensembles of SST-forced models. In this case we compute pattern correlations of the model 200-mb height anomalies with the observed winter 2013/14 height anomaly. Since we do this for all the ensemble members for each year we end up with a distribution of pattern correlation coefficients shown in Fig. 5 in terms of the 25th and 75th percentiles. Figure 5 also shows the pattern correlation coefficient for the ensemble mean height anomaly. Pattern correlation with the observed winter 2013/14 height anomaly reveals how well the models simulated this event. CFSv2, ECHAM4.5, and GEOS-5 had correlation coefficients above 0.5 while those of CCM3 and ESRL-GFSv2 are notably low.[1] The model time series show that for many models there are pattern correlations with the observed winter 2013/14 height anomaly that are higher than that for the model simulation of winter 2013/14. That is, for those models, past SST anomaly patterns forced an atmospheric response more akin to the observed winter 2013/14 than the SST anomaly in that winter itself did. For all the models there are frequently recurring patterns that are akin to that in winter 2013/14 but none that match so closely that the pattern correlation exceeds 0.8.

To examine how well the observed and modeled time histories of height anomalies akin to winter 2013/14 match, in Fig. 6 we plot the time series of the pattern correlation coefficients of 1) NCEP–NCAR reanalysis (repeated from Fig. 4) and 2) the model ensemble means with the NCEP–NCAR winter 2013/14 pattern. The correlation coefficients between the time series pairs are noted on the plots. With the exception of CCM3, where the correlation is only significant at the 90% level, all the model-reanalysis time series are correlated at greater than the 95% level. Since the model ensemble means represent SST-forced variations, this makes a strong case that the observed time history of height anomalies akin to those in winter 2013/14 was strongly influenced by SST variations.

The shorter model simulations are consistent with the NCEP and ERA-Interim reanalyses in showing no trend in occurrence of patterns akin to winter 2013/14. However, the three century-scale integrations with CAM5, CCM3, and GEOS-5 do show multidecadal time scale trends toward height anomaly patterns more akin to winter 2013/14 (Fig. 6). These trends are significant at the 95% level. In the case of GEOS-5 the model simulates the observed pattern of winter 2013/14 very well, and, hence, this model in particular supports the indication from the observations-based 20CR reanalysis that there has been a steady trend toward a high pressure ridge during winters at the North American west coast and that this is occurring as a response to the change in SST over this period.

2) ASSOCIATION OF WEST COAST RIDGES WITH GLOBAL SST ANOMALIES

The particular circulation anomaly of winter 2013/14 has been associated with the tropical SST forcing (seen in Fig. 4). The analysis just presented provides a way to assess, in observations and models, how circulation anomalies akin to those of winter 2013/14 relate to SST anomalies. This can be done by regressing global SST anomalies on the time series of pattern correlation coefficients. The period used was 1979 to 2014 since this is common to all reanalyses and model simulations. The resulting regression coefficients, which indicate the strength of the relation to SST, are shown in Fig. 7 with colors applied where the relation is significant at the

[1] In the case of CCM3, this is shown by Seager and Henderson (2016) to be partly a consequence of forcing the model with Hadley Centre SST data while the same model response to NOAA ERSSTv4 data is more realistic.

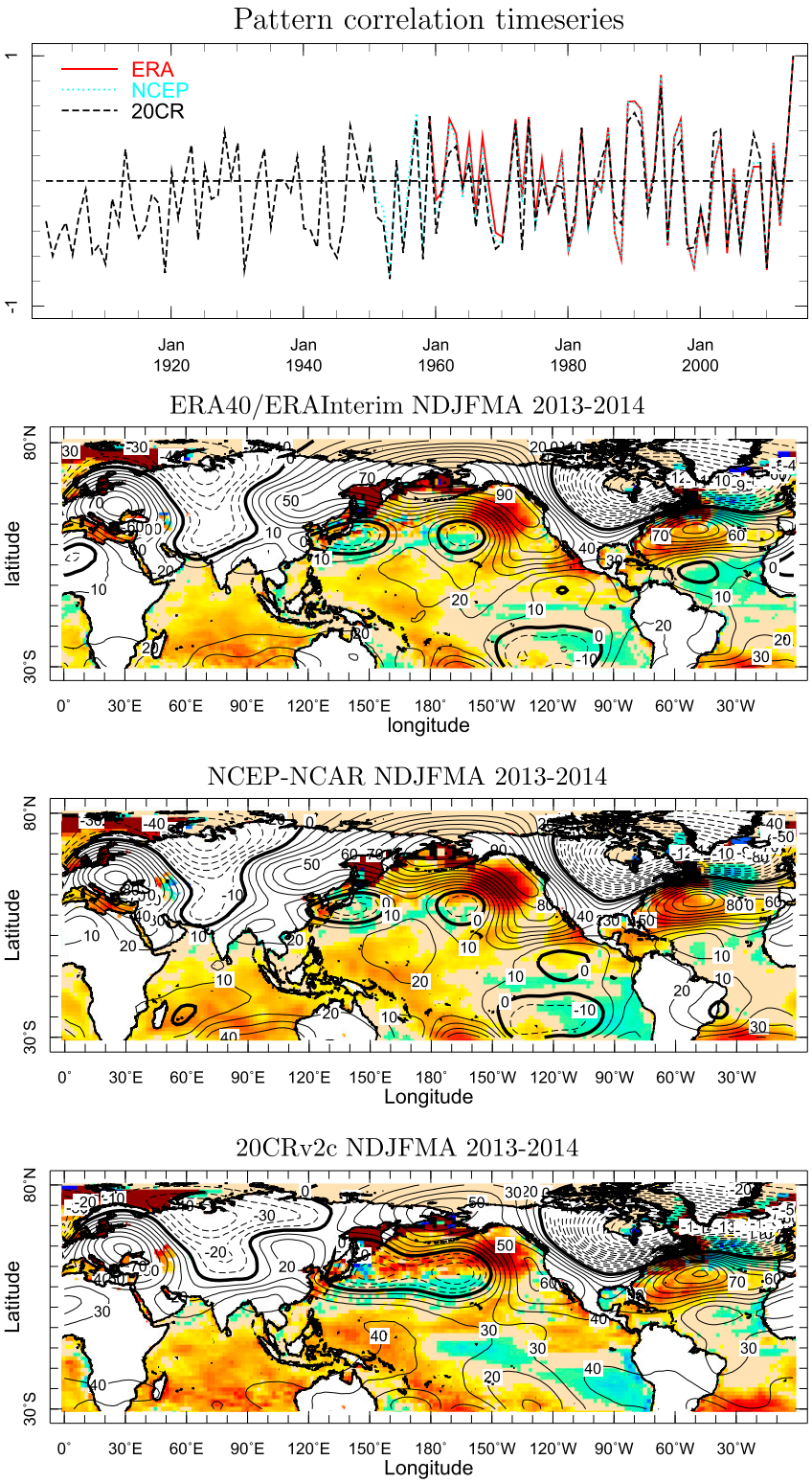

FIG. 4. Time series of the pattern correlation between the November–April 2013/14 200-mb geopotential height anomaly north over 20°−80°N, 120°E − 40°W and that of all other November–April winters within three reanalyses: NCEP–NCAR, ERA-40/ERA-Interim, and 20CR. By construction the pattern correlation for 2013/14 is 1. The winter 2013/14 height anomaly (contours; m) and SST anomaly (colors over ocean; K) are shown below for three reanalyses.

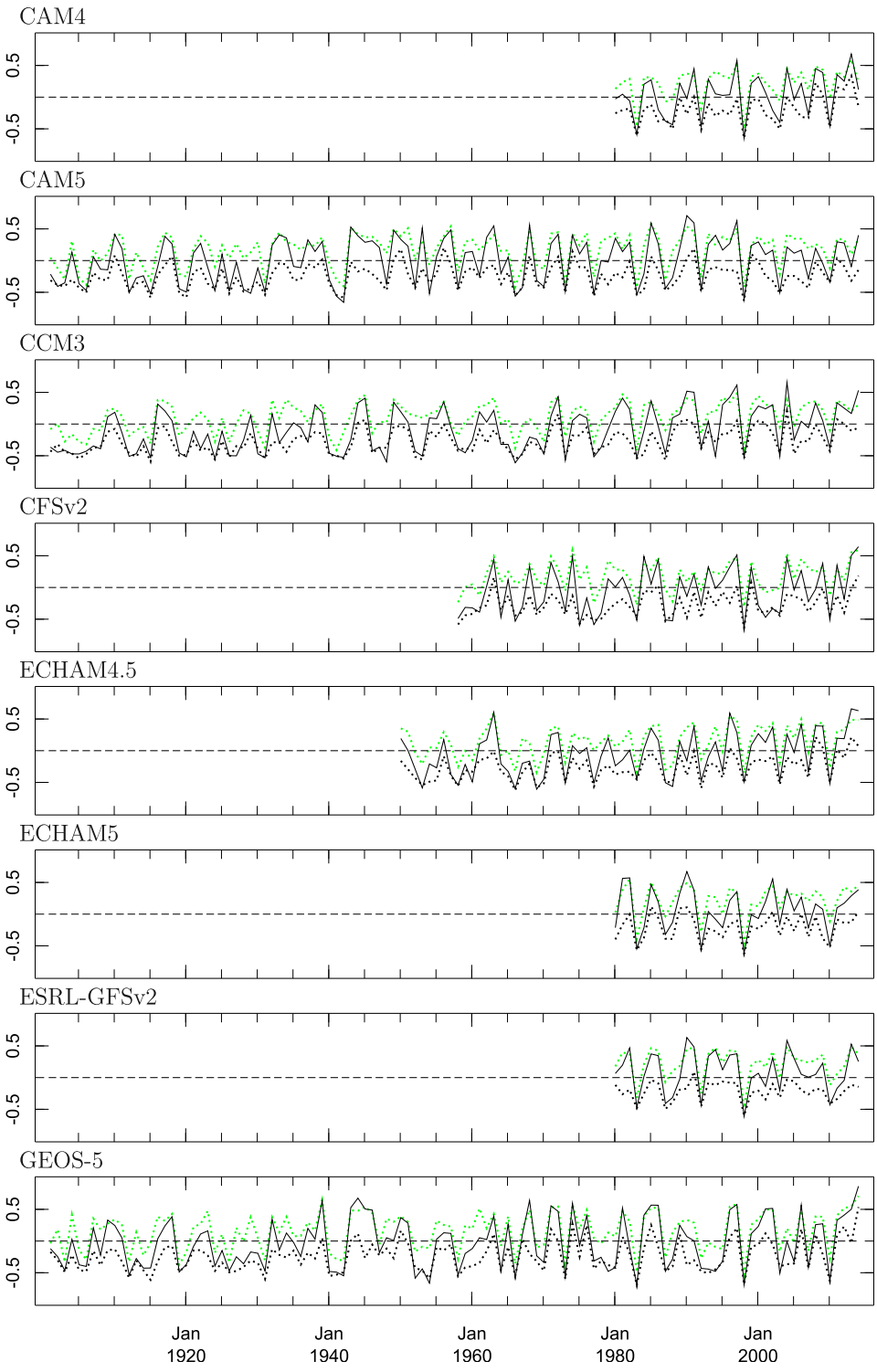

FIG. 5. Time series of the pattern correlation between the November–April 2013/14 200-mb geopotential height anomaly over 20°−80°N, 120°E − 40°W as given by the NCEP–NCAR reanalysis and that of November–April winters within eight SST-forced atmosphere models. Shown are the value for the model ensemble mean (black), representing the pattern correlations for the SST-forced response, and the 25th and 75th percentiles of the distribution of pattern correlations across the ensemble members (green). The values for 2013/14 are measures of how well the modeled height anomaly matches that which actually occurred as a consequence of SST forcing plus internal atmosphere variability (members) and SST forcing alone (mean).

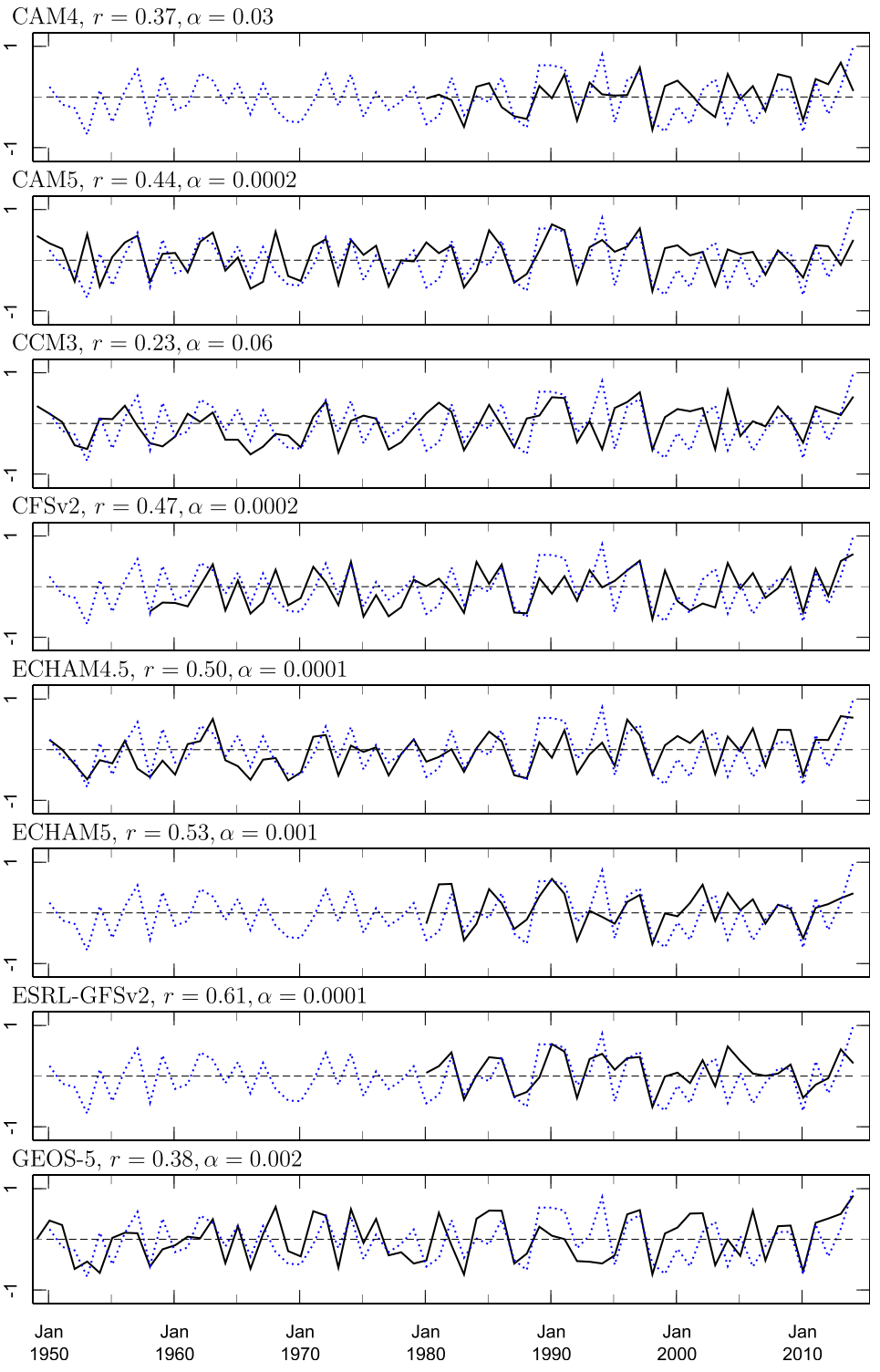

FIG. 6. Time series of the pattern correlation between the November–April 2013/14 200-mb geopotential height anomaly over 20°−80°N, 120°E − 40°W as given by the NCEP–NCAR reanalysis and that of November–April winters within the NCEP–NCAR reanalysis itself (each panel; blue dots; value of 1 during winter 2013/14) and the eight SST-forced atmosphere models (solid lines). The correlation coefficient between the two time series and the significance level are shown next to the model name above each panel.

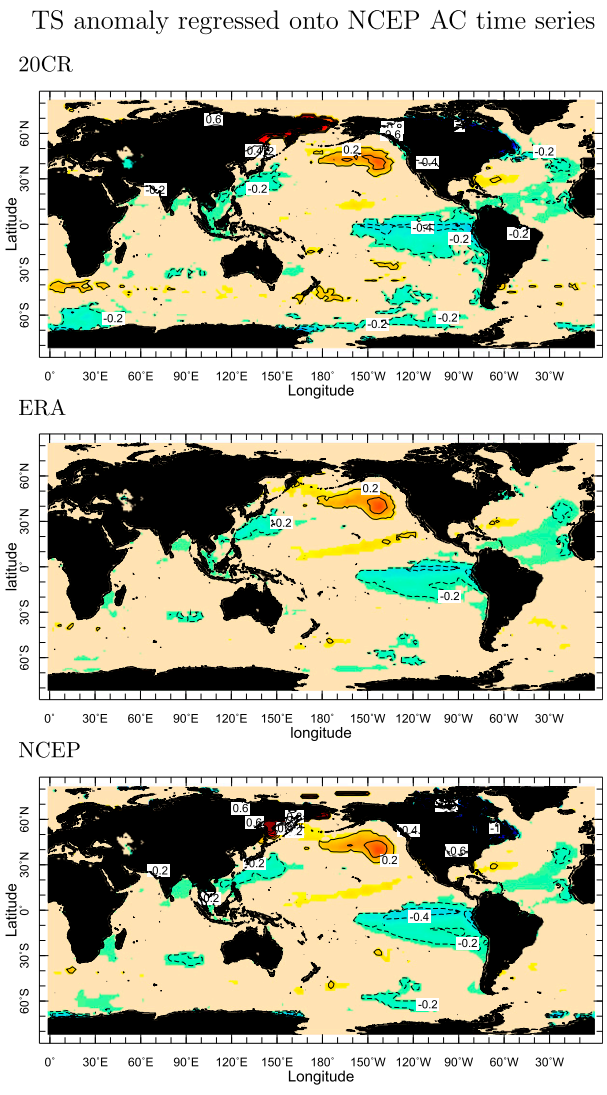

FIG. 7. Regression of the time series of the pattern correlation between the November–April 2013/14 200-mb geopotential height anomaly over 20°–80°N, 120°E–40°W and that of all November–April winters with SST anomalies for three reanalyses and the 1979 to 2014 period. Colors are applied for where significant at the 95% level. Units are K.

95% level. Most notable is the association in each of the west coast ridge with an increased west–east SST gradient across the tropical Pacific Ocean with a hint of warm in the western Pacific warm pool and cool along the Equator in the central to eastern Pacific. The SST anomalies in the North Pacific Ocean are consistent with being forced by the atmosphere via surface flux and wind anomalies and, hence, a response to the ridge rather than driving (Bond et al. 2015; Hartmann 2015; Seager and Henderson 2016). The ridge-associated SST pattern is consistent with the results of Seager et al. (2015), who, using the same model ensembles analyzed here, identified this increased SST gradient–west coast ridge association as the third SST-forced mode in an empirical orthogonal function analysis of the model ensemble means.

Figure 8 then shows the regression of the time series of observed–model pattern correlation coefficients (from Fig. 6) with the SST forcing for the eight SST-forced models. The SST anomaly patterns are very similar to those for the reanalyses and again confirm that height anomaly patterns akin to the winter 2013/14 anomaly are favored by an enhanced west–east SST gradient across the tropical Pacific Ocean.

This SST anomaly pattern is not simply La Niña. Within the observations, the correlation coefficient between the time series of the pattern correlation and the Niño-3.4 (SST anomaly over 5°S − 5°N, 170°−130°W) index maximizes at 0.41 with Niño-3.4 leading by one year. It is possible that the ridge-associated SST pattern does occur as part of an irregular ENSO cycle (e.g., see Wang et al. 2014), but further investigation of that matter is left aside for now. All the multiple lines of evidence indicate a connection of the ridge to a pattern of increased SST gradient across the Indo-Pacific Oceans.

3) Lack of observational evidence of forcing of California precipitation by sea ice variability and change

Arctic sea ice loss over recent decades is a dramatic feature of climate change and is almost certainly driven in important measure by rising GHGs [see Semenov et al. (2015) for a recent review and discussion of this enormous literature]. Such dramatic change has led to reasonable suspicion that it has influenced climate variability and change in the Arctic and in northern subpolar and midlatitudes. Screen et al. (2015) used model simulations that isolated the influence of Arctic sea ice loss to argue the case for widespread cross–Northern Hemisphere influences on temperature and precipitation extremes. However, the west coast of North America was one area where they did not see an influence. In contrast, Lee et al. (2015) argue, also based on model simulations, that Arctic sea ice loss did play a role in creating the extreme circulation anomalies over the North Pacific and North America in winter 2013/14, by extension implicating human-driven climate change in the California drought. Of course the CMIP5 models analyzed above do have reductions in Arctic sea ice both for the current and future decades relative to the recent past (Semenov et al. 2015) but nonetheless show no tendency for west coast ridging or increased drought risk in California. However, this could be because of model error or masking of a sea ice–induced change by other processes. Therefore we turn to the observational record

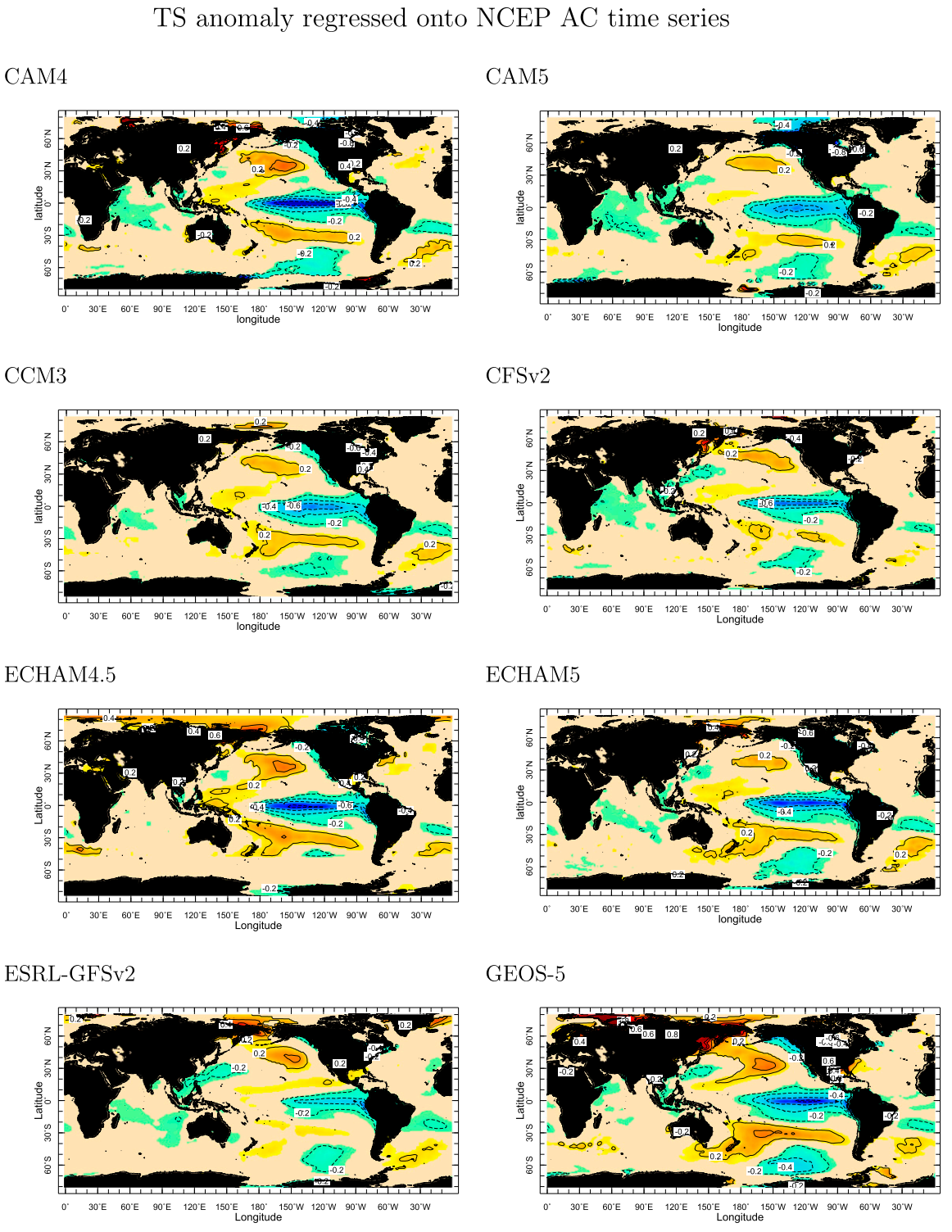

FIG. 8. As in Fig. 7, but for the SST-forced atmosphere model simulations 37

and assess whether there is any evidence based on past change and interannual variability for California winter precipitation to be sensitive to changes in Arctic sea ice area.

First we plot together the history of California winter precipitation and Arctic sea ice anomaly in terms of area covered by ice at the annual minimum month of September and also as the November through April

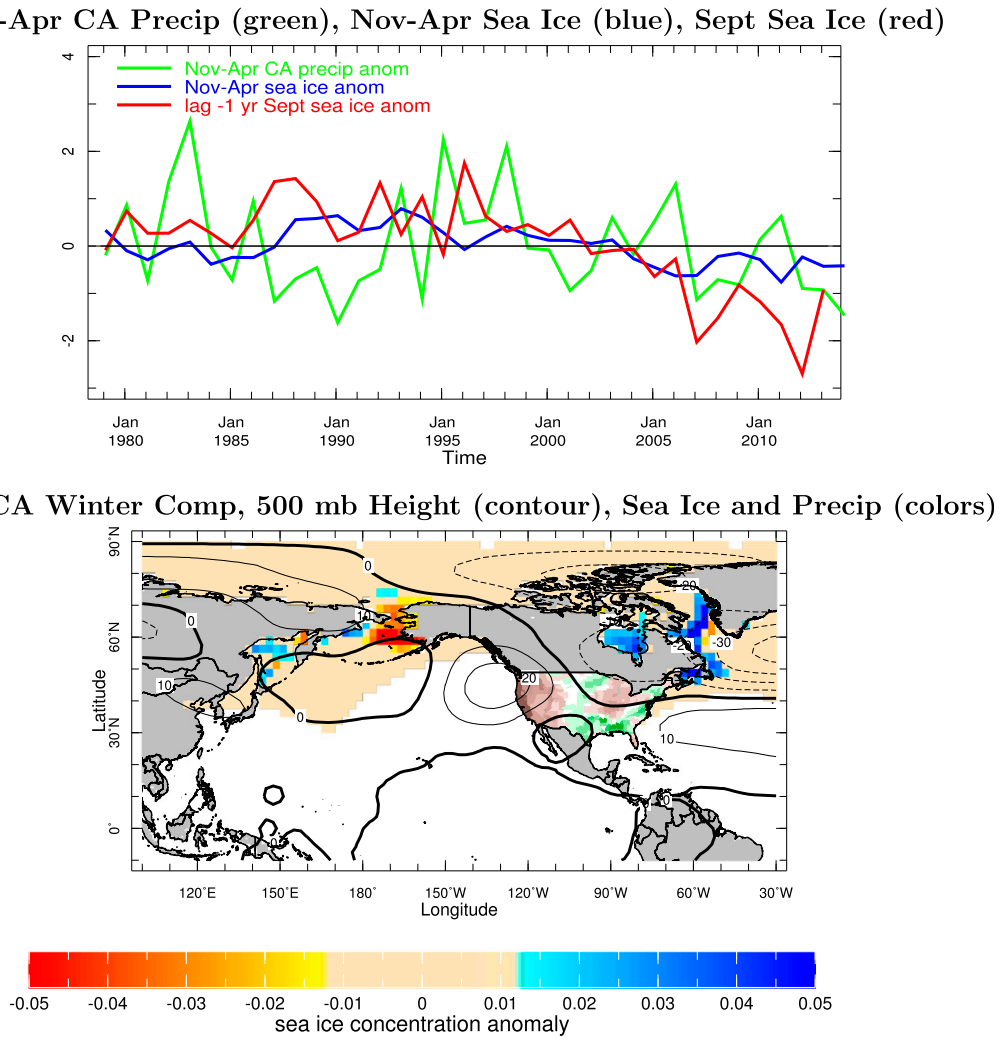

FIG. 9. Time series of (top) November–April California precipitation with Northern Hemisphere sea ice anomaly for concurrent six-month average and the prior September and U.S. precipitation, 500-mb heights, and sea ice cover anomalies composited over the driest 15% of California winters during the 1979 to 2015 period.

winter average (Fig. 9, top). While all three are of course negative during the drought years there is no year to year relationship between these quantities. Next we composite 200-mb height anomalies, U.S. precipitation, and sea ice concentration for, during the period covered by sea ice data, the driest 15% of California winters and subtract the climatological winter values (Fig. 9, bottom). As in Seager et al. (2015), the composites show that when California is dry the entire western third of the United States tends to be dry and that there is a high pressure ridge located immediately off the west coast, which does not appear to be connected to a tropically sourced wave train. There also tends to be a trough over the North Atlantic, similar to winter 2013/14. There are notable localized sea ice concentration anomalies with increased ice in the Sea of Okohtsk, reduced ice in the Bering Sea, and increased ice in Hudson Bay and Labrador Sea, though the anomalies are small. These ice anomalies are consistent with atmospheric forcing. The Sea of Okhotsk and Hudson Bay/Labrador Sea anomalies appear under northerly flow that would favor cold advection and increased ice. The Bering Sea anomaly appears under easterly flow that would drive ice offshore. As shown by Seager et al. (2015), the dry California winters are also associated with North Pacific SST anomalies forced by the atmospheric wave train and the sea ice anomalies appear part of this feature rather than as causal drivers of the atmospheric circulation anomalies. These analyses do not support the idea that variations in sea ice extent influence the prevalence of west coast ridges or dry winters in California.

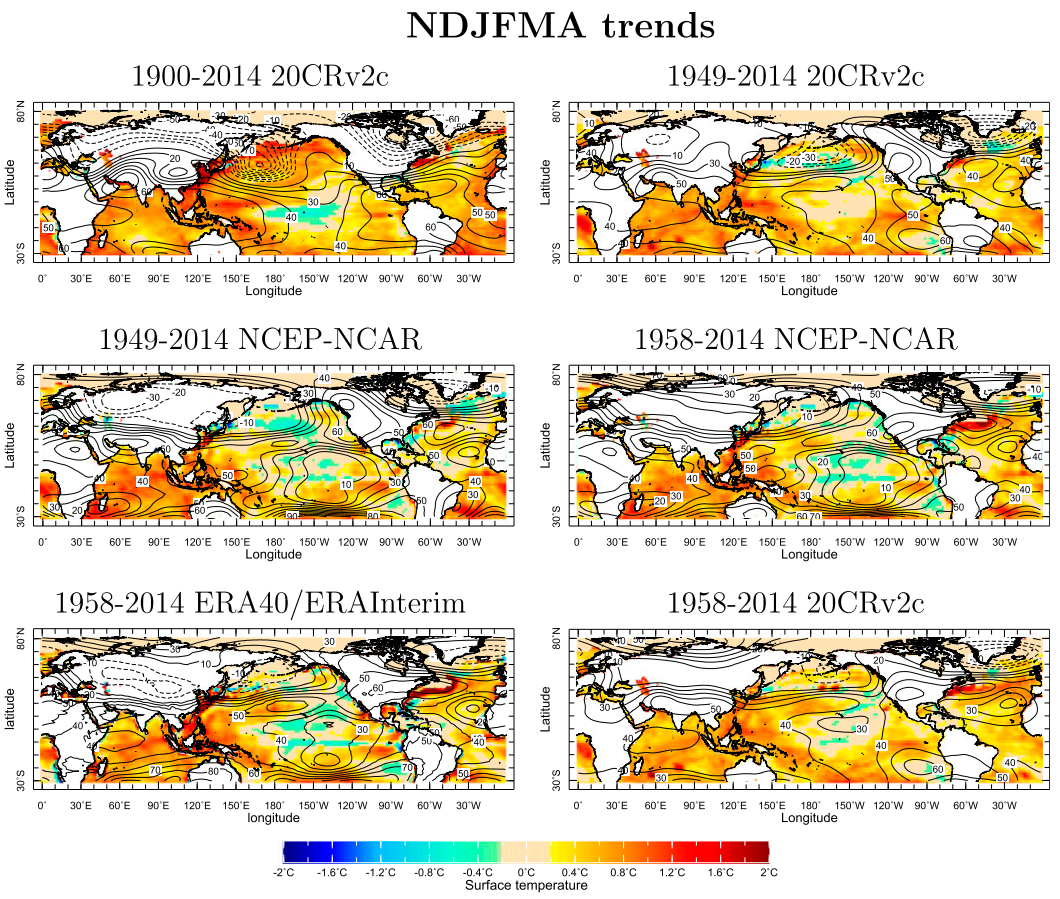

FIG. 10. Trends in November–April 200-mb geopotential height (contours; m) and associated SST (colors; K) fields from the 20CR, NCEP–NCAR, and ERA-40/ERA-Interim reanalyses for all possible complete periods (1900–2014, 1949–2014, 1958–2014) with multiple realizations from different reanalyses as allowed.

4) LONG-TERM TRENDS IN SSTS AND CIRCULATION

On the basis of the above analysis we conclude that the occurrence of persistent ridges at the west coast is more connected to SST anomalies than it is to sea ice anomalies. The CMIP5 model ensemble lends no support to the idea that ridge-inducing SST patterns become more likely as a result of rising GHGs. However, the models could be wrong so we next examine whether trends in observed SSTs lend any support to this idea. Trends were computed by straightforward linear least squares regression. Trends in November to April SST from a variety of SST data products are shown in Fig. 10. The trends are shown for the entire period of the atmospheric reanalyses they were used with but with two exceptions. The 20CR trends are from 1900 on because of the paucity of surface pressure data in the nineteenth century and, for ERA-40/ERA-Interim, surface temperature is not made available and we use 2-m air temperature instead. The trends are plotted for three time periods: 1900 to 2014 (20CR), 1948 to 2014 (20CR and NCEP–NCAR), and 1958 to 2014 (20CR, NCEP–NCAR, and ERA-40/ERA-Interim). The 200-mb height trends for the same periods within the reanalyses that made use of the SST products are also shown, and in Fig. 11 we show the reanalysis precipitation trends.

A number of features stand out in these trends regardless of the time period used.

(i) Amid near-ubiquitous warming of the oceans the central equatorial Pacific stands out as a place that has not warmed.
(ii) The west–east SST gradient across the tropical Pacific has strengthened as the west Pacific has warmed.
(iii) Increased reanalysis precipitation over the Indian Ocean–Maritime Continent–tropical west Pacific and reduced reanalysis precipitation over the central equatorial Pacific Ocean were found.
(iv) Tropical geopotential heights have increased at all longitudes.

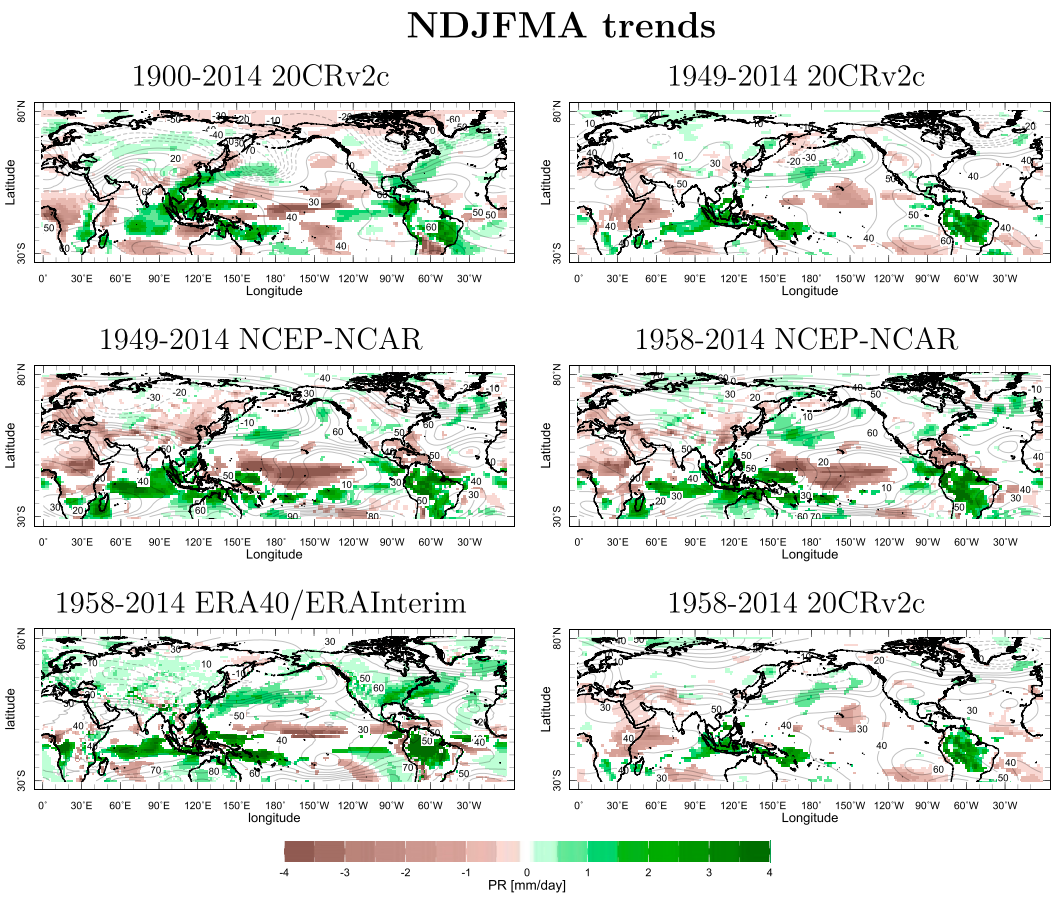

FIG. 11. As in Fig. 10, but for precipitation (mm day^{-1}). Colors are shown only where the trend is significant at the 5% level.

(v) A trend toward a localized high pressure ridge extending from the subtropics toward Alaska across western North America.

These associations in the trends—a strengthened west–east SST gradient across the tropical Pacific and localized high pressure at the North American west coast—are in line with every piece of evidence based on observations and SST-forced models presented so far that there is a connection between drought-inducing circulation anomalies and tropical Pacific SSTs. The mediating influence is seen in the precipitation trends that show enhanced zonal gradients of tropical Indo-Pacific precipitation and a marked increase centered over the Maritime Continent region. These associations are evident regardless of period over which the trend is computed. If the height trends were strongly influenced by internal atmosphere variability we would not expect such consistency of trends sampled over different periods. However, the pattern of the height trend is not the same as that of the west coast ridge of winter 2013/14 (Fig. 4). The low in the trend centered over the Aleutian Islands is notably in contrast to the high here during winter 2013/14. The trend and the winter 2013/14 pattern do however share high heights over the eastern North Pacific–west coast–western North America region. Hence, the trend could aid in building up a west coast ridge. Precipitation trends over California are not consistent across periods or reanalyses, but the observed precipitation over California shows no clear long-term trends with the history to date dominated by natural variability on a wide range of time scales (Seager et al. 2015).

If the height trends are indeed related to the SST trends we would hope they are reproduced in SST-forced atmosphere models. In Fig. 12 we therefore show the height and SST trends for the same periods as shown in Fig. 11 and, for each period, averaging across all the models available. The SST trends are of course very similar to those in the reanalyses differing only due to use of different SST products. The height trends forced by the SST trends have highs across the tropics

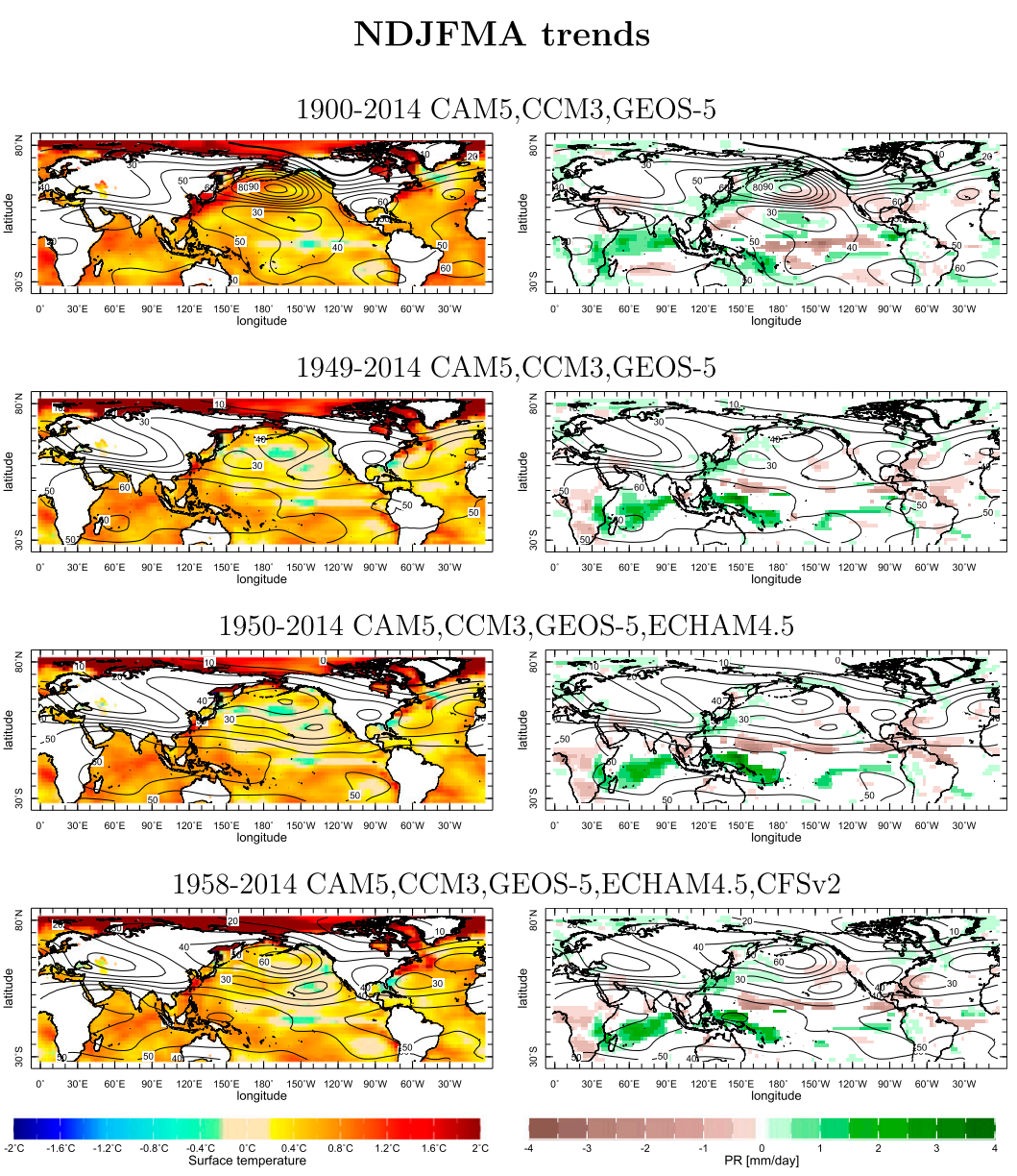

FIG. 12. As in Figs. 10 and 11, but for the multimodel average of the eight SST-forced atmosphere model simulations with (left) height and SST trends and (right) precipitation trends. The precipitation trends are colored only where significant at the 5% level.

and over the extratropical North Pacific and southern North America. The main difference of interest in this context is that the reanalysis trends have a localized ridge over western North America in contrast to over the North Pacific for the SST-forced models. The individual ensemble members do not provide any that match reanalysis trends better (not shown), which is consistent with the reanalysis and modeled trends not being strongly influenced by internal atmospheric variability.

c. *Idealized area-SST modeling to identify SST patterns best able to force a west coast ridge*

This presents us with an apparent contradiction. The observational analysis indicates a long-term trend toward a ridge over western North America that is hard to explain in terms of internal atmosphere variability, but the SST-forced models instead produce a trend to high heights over the North Pacific Ocean. However, the sensitivity of circulation in the Pacific–North American sector to small

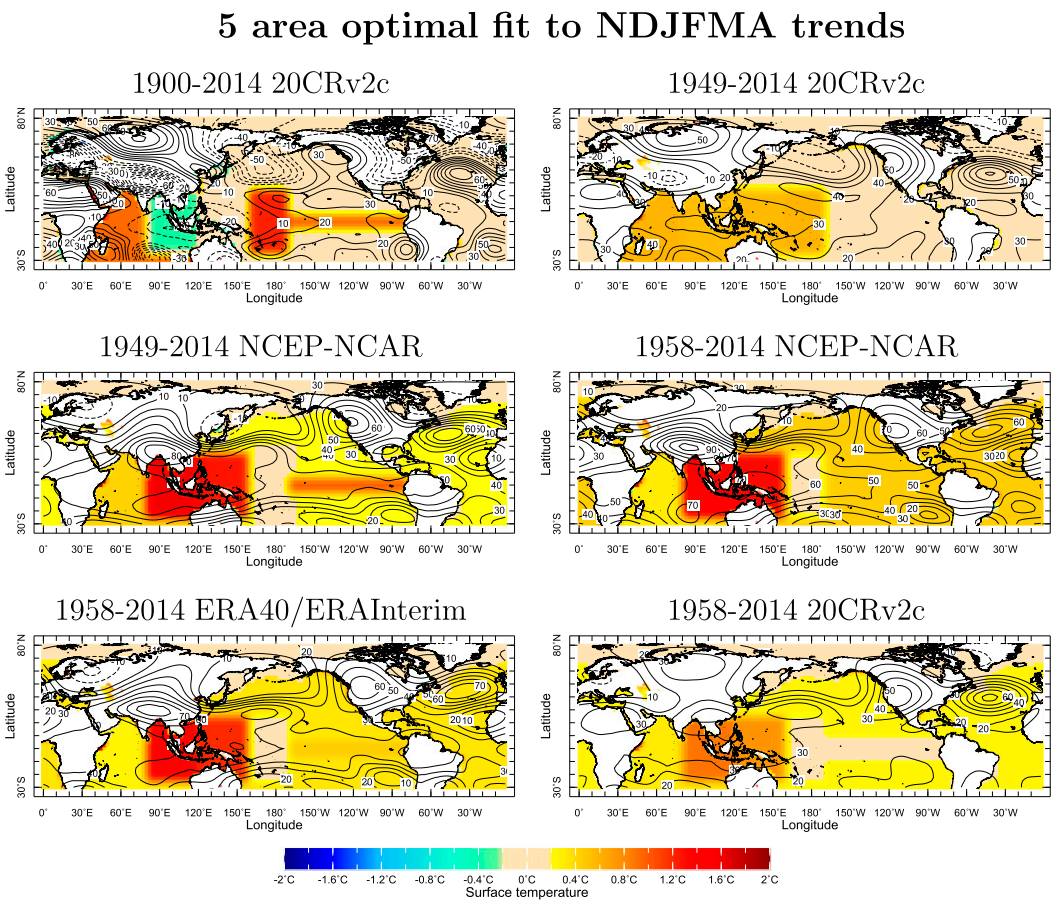

FIG. 13. The 200-mb height anomalies (contours) and associated SST forcing (colors) constructed as the constrained linear combination of height responses to area-SST experiments that best match the reanalysis trends in Fig. 11. Units are m and K.

changes in tropical SSTs shown by Seager and Henderson (2016) in the context of winter 2013/14 gives one cause to wonder about the SST-forced model results. There are considerable uncertainties in the SSTs within the observational datasets (see, e.g., Huang et al. 2015). This is seen in Fig. 10 where the SST trends in three different reanalyses that used different SST data for the common 1958 to 2014 period are shown. While the broad features are similar and so are many of the details, the greater warming in the Maritime Continent region within ERA-40/ERA-Interim compared to NCEP–NCAR and 20CRv2c is clear. Given the uncertainties in the SST data there are an infinite number of other ''observed'' SST trends that are plausible, and it is possible that they will be different enough to matter for the atmospheric circulation response in the Pacific–North American sector.

Hence, as Seager and Henderson (2016) did to examine the causes of the winter 2013/14 west coast ridge, we use idealized modeling here to understand the heights trend. For each of the height trends shown in Fig. 10 we calculate the optimal linear combination (with no constraint on amplitude or sign) of tropical Indian and Pacific Ocean and global area-SST height responses that best matches the height trend (by minimizing the area-weighted sum of squared differences between model and reanalysis heights over 20°–80°N, 120°E–40°W). The weights in the linear combination are then used with the area-SST anomalies to compute the associated optimal SST forcing field. Results are shown in Fig. 13. The constructive modeling approach allows quite close matches in pattern and amplitude to the reanalysis height trends despite the very limited set of idealized area-SST anomalies, whereas the real height trends are influenced by nuanced changes in tropical SSTs as well as surface conditions everywhere else and changes in radiative forcing. That said, it is interesting that, of all the possible SST anomaly patterns, signs, and amplitudes the optimization methodology allows, it decides the best fit for each period and target reanalysis

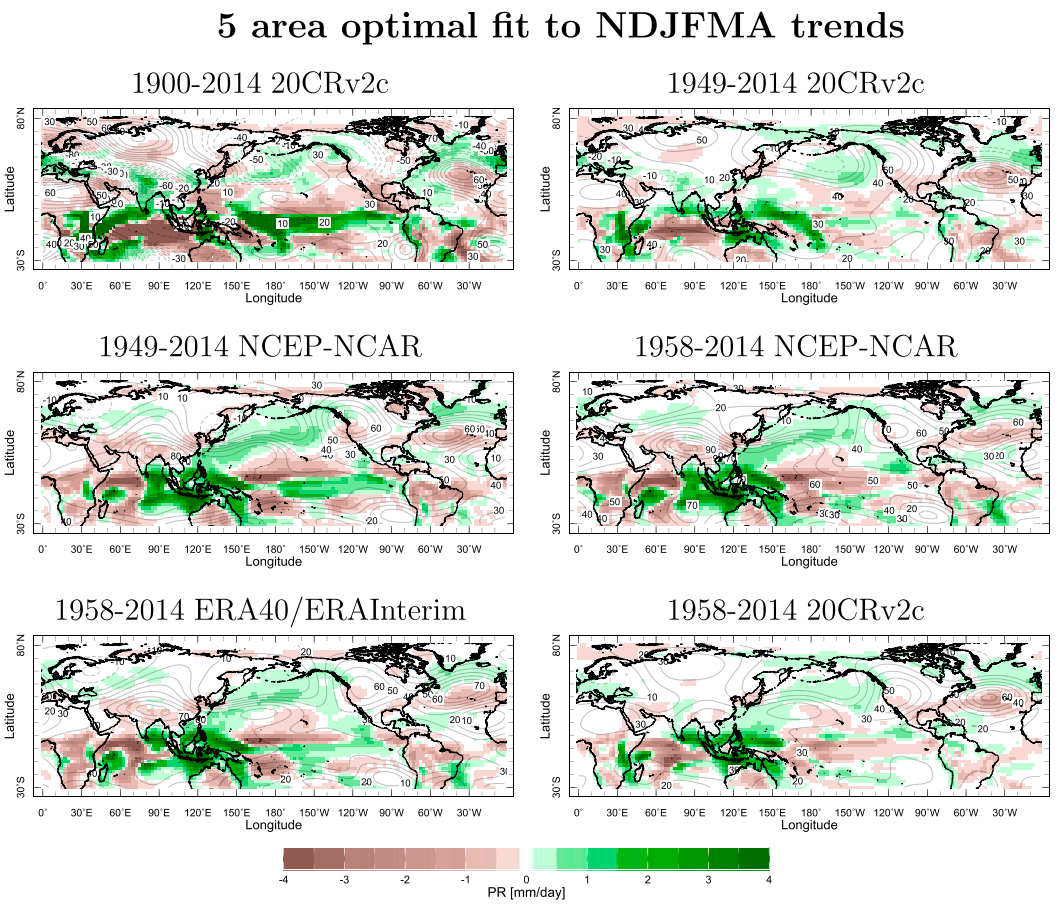

FIG. 14. As in Fig. 14, but for the precipitation response.

trend comes from having the warmest anomalies in the Indian Ocean–Maritime Continent–western Pacific region. For the most recent trends the height trend is better matched if the warm Indo–west Pacific SSTs are placed within overall warmer global SSTs. This pattern of SST change does bear some similarity to the actual SST trends in the reanalyses. The precipitation patterns derived from the optimization (Fig. 14) also have the high precipitation over the tropical Indo–west Pacific seen in the reanalyses and consistent with the underlying SST pattern. In summary, the observed (as in the reanalysis) coarrangement of heights, SSTs, and precipitation is similar in essence to that which an unconstrained optimization indicates is best able to account for a trend toward a west coast ridge. The optimized pattern also has dry conditions over California.

4. Conclusions and discussion

We have examined whether there is any evidence, observational and/or model based, that the precipitation decline that drove the California drought was contributed to by human-driven climate change. Findings are as follows:

- The CMIP5 model ensemble provides no evidence for mean drying or increased prevalence of dry winters for California or a shift toward a west coast ridge either in the mean or as a more common event. They also provide no evidence of a shift in tropical SSTs toward a state with an increased west–east SST gradient that has been invoked as capable of forcing a west coast ridge and drought.
- Analysis of observations-based reanalyses shows that west coast ridges, akin to that in winter 2013/14, are related to an increased west–east SST gradient across the tropical Pacific Ocean and have repeatedly occurred over past decades though as imperfect analogs.
- SST-forced models can reproduce such ridges and their connection to tropical SST anomalies.
- Century-plus-long reanalyses and SST-forced models indicate a long-term trend toward circulation anomalies more akin to that of winter 2013/14.
- The trends of heights and SSTs in the reanalyses also show both an increased west–east SST gradient and a 200-mb ridge over western North America that, in

terms of association between ocean and atmospheric circulation, matches those found via the other analyses on interannual time scales.
- However, SST-forced models when provided the trends in SSTs create a 200-mb ridge over the central North Pacific and, in general, a circulation pattern that cannot be said to truly match that in reanalyses.

So can a case be made that human-driven climate change contributed to the precipitation drop that drives the drought? Not from the simulations of historical climate and projections of future climate of the CMIP5 multimodel ensemble. These simulations show no current or future increase in the likelihood or extremity of negative precipitation, precipitation minus evaporation, west coast ridges, or ridge-forcing tropical SST patterns. However, when examining the observational record a case can be made that the climate system has been moving in a direction that favors both a ridge over the west coast, which has a limited similarity to that observed in winter 2013/14, the driest winter of the drought, and a ridge-generating pattern of increased west–east SST gradient across the tropical Pacific Ocean with warm SSTs in the Indo–west Pacific region. This observations-based argument then gets tripped up by SST-forced models, which know about the trends in SST but fail to simulate a trend toward a west coast ridge. On the other hand, idealized modeling indicates that preferential warming in the Indo–west Pacific region does generate a west coast ridge.

These results collectively are both tantalizingly suggestive that the observed SST and ridge trends are related and part of a long-term change driven from the tropics and annoyingly inconclusive. The various parts of the argument could be brought into consistency if either the SST trends in the reanalyses were in some way in error and the height trend could be produced as a response to different—though equally plausible given data uncertainties—SST trends or if the atmosphere models have common biases in the atmosphere response to imposed tropical SSTs.

The possibility that the trends in the tropical Pacific west–east SST gradient, even on multidecadal to centennial time scales, are a result of natural climate variability should not be dismissed (Karnauskas et al. 2012). However, if these trends are forced then an argument for a human role in the precipitation drop over California would go as follows:

(i) Rising greenhouse gases increased downward longwave radiative flux into the oceans.
(ii) The Indian and west tropical Pacific Oceans, where net ocean heat flux divergence is small, warm up to compensate the extra longwave heating with increased latent heat loss. In the east and central Pacific cold tongue much of radiative heat flux gain is diverged away from the equator in the upwelling meridional overturning circulation and the ocean warms less than it does farther west (Clement et al. 1996; Cane et al. 1997).
(iii) The west–east SST gradient strengthens and drives an atmospheric circulation response that places a ridge at the west coast of North America.
(iv) The ridge shields the west coast from Pacific storms and suppresses precipitation.

Palmer (2014), making a similar case, has also drawn attention to how changing tropical SST gradients under the influence of rising greenhouse gases could have favored the North American east coast trough and cold, snowy winter of 2013/14 that went along with the west coast ridge and worst year of the California drought. To make the argument we outline above requires rejecting the CMIP5 ensemble as a guide to how tropical climate responds to increased radiative forcing since this tropical ocean response is at odds with what they do. To do so follows in the footsteps of Kohyama and Hartmann (2017, p. 4248), who correctly point out that ''El Niño–like mean-state warming is only a 'majority decision' based on currently available GCMs, most of which exhibit unrealistic nonlinearity of the ENSO dynamics'' (see also Kohyama et al. 2017). The implications of changing tropical SST gradients would extend far beyond just California and include most regions of the world sensitive to ENSO-generated climate anomalies. We believe that the current state of observational information, analysis of it, and climate modeling does not allow a confident rejection of the CMIP5 model responses and/or a confident assertion of human role in the precipitation drop of the California drought. We also believe that for the same reasons a human role cannot be excluded.

Acknowledgments. This work was supported by NOAA Award NA10OAR4310232 and NSF Awards AGS-1401400, AGS-1243204, and OCE-16-57209 and World Surf League P.U.R.E. We thank Dong-Eun Lee for generating the CAM5 ensemble. This article is Lamont-Doherty Earth Observatory contribution number 8164.

REFERENCES

Berg, N., and A. Hall, 2015: Increased interannual precipitation extremes over California under climate change. *J. Climate*, **28**, 6324–6334, https://doi.org/10.1175/JCLI-D-14-00624.1.

Bond, N. E., M. F. Cronin, H. Freeland, and N. Mantua, 2015: Causes and impacts of the 2014 warm anomaly in the NE Pacific. *Geophys. Res. Lett.*, **42**, 3414–3420, https://doi.org/10.1002/2015GL063306.

Cane, M. A., A. C. Clement, A. Kaplan, Y. Kushnir, D. Pozdnyakov, R. Seager, S. E. Zebiak, and R. Murtugudde, 1997: Twentieth-century sea surface temperature trends. *Science*, **275**, 957–960, https://doi.org/10.1126/science.275.5302.957.

Clement, A. C., R. Seager, M. A. Cane, and S. E. Zebiak, 1996: An ocean dynamical thermostat. *J. Climate*, **9**, 2190–2196, https://doi.org/10.1175/1520-0442(1996)009<2190:AODT>2.0.CO;2.

Compo, G., and Coauthors, 2011: The Twentieth Century Reanalysis Project. *Quart. J. Roy. Meteor. Soc.*, **137**, 1–28, https://doi.org/10.1002/qj.776.

Dee, D., and Coauthors, 2011: The ERA-Interim Reanalysis: Configuration and performance of the data assimilation system. *Quart. J. Roy. Meteor. Soc.*, **137**, 553–597, https://doi.org/10.1002/qj.828.

Hartmann, D. L., 2015: Pacific sea surface temperature and the winter of 2014. *Geophys. Res. Lett.*, **42**, 1894–1902, doi:10.1002/2015GL063083.

Huang, B., and Coauthors, 2015: Extended reconstructed sea surface temperature version 4 (ERSST.v4). Part I: Upgrades and intercomparisons. *J. Climate*, **28**, 911–930, https://doi.org/10.1175/JCLI-D-14-00006.1.

Kalnay, E., and Coauthors, 1996: The NCEP/NCAR 40-Year Reanalysis Project. *Bull. Amer. Meteor. Soc.*, **77**, 437–471, https://doi.org/10.1175/1520-0477(1996)077<0437:TNYRP>2.0.CO;2.

Karnauskas, K. B., J. E. Smerdon, R. Seager, and J. F. González-Rouco, 2012: A Pacific centennial oscillation predicted by coupled GCMs. *J. Climate*, **25**, 5943–5961, https://doi.org/10.1175/JCLI-D-11-00421.1.

Kelley, C. P., S. Mohtadi, M. A. Cane, R. Seager, and Y. Kushnir, 2015: Climate change in the Fertile Crescent and implications of the recent Syrian drought. *Proc. Natl. Acad. Sci. USA*, **112**, 3241–3246, https://doi.org/10.1073/pnas.1421533112.

Kistler, R., and Coauthors, 2001: The NCEP–NCAR 50-Year Reanalysis: Monthly means CD-ROM and documentation. *Bull. Amer. Meteor. Soc.*, **82**, 247–267, https://doi.org/10.1175/1520-0477(2001)082<0247:TNNYRM>2.3.CO;2.

Kohyama, T., and D. L. Hartmann, 2017: Nonlinear ENSO warming suppression (NEWS). *J. Climate*, **30**, 4227–4251, https://doi.org/10.1175/JCLI-D-16-0541.1.

——, ——, and D. S. Battisti, 2017: La Niña–like mean-state response to global warming and potential oceanic roles. *J. Climate*, **30**, 4207–4225, https://doi.org/10.1175/JCLI-D-16-0441.1.

Lee, M.-Y., C.-C. Hong, and H.-H. Hsu, 2015: Compounding effects of warm sea surface temperature and reduced sea ice on the extreme circulation over the extratropical North Pacific and North America during the 2013–14 boreal winter. *Geophys. Res. Lett.*, **42**, 1612–1618, https://doi.org/10.1002/2014GL062956.

Li, G., S.-P. Xie, Y. Du, and Y. Luo, 2016: Effects of excessive equatorial cold tongue bias on the projections of tropical Pacific climate change. Part I: The warming pattern in CMIP5 multi-model ensemble. *Climate Dyn.*, **47**, 3817–3831, https://doi.org/10.1007/s00382-016-3043-5.

Neelin, J. D., B. Langenbrunner, J. E. Meyerson, A. Hall, and N. Berg, 2013: California winter precipitation change under global warming in the coupled model intercomparison project phase 5 ensemble. *J. Climate*, **26**, 6238–6256, https://doi.org/10.1175/JCLI-D-12-00514.1.

Palmer, T. N., 2014: Record-breaking winters and global climate change. *Science*, **344**, 803–804, https://doi.org/10.1126/science.1255147.

Screen, J. A., C. Deser, and L. Sun, 2015: Projected changes in regional climate extremes arising from Arctic sea ice loss. *Environ. Res. Lett.*, **10**, 084006, doi:10.1088/1748–9326/10/8/084006.

Seager, R., and N. Henderson, 2016: On the role of tropical ocean forcing of the persistent North American West Coast ridge of winter 2013/14. *J. Climate*, **29**, 8027–8049, https://doi.org/10.1175/JCLI-D-16-0145.1.

——, N. Naik, and L. Vogel, 2012: Does global warming cause intensified interannual hydroclimate variability? *J. Climate*, **25**, 3355–3372, https://doi.org/10.1175/JCLI-D-11-00363.1.

——, M. Hoerling, S. Schubert, H. Wang, B. Lyon, A. Kumar, J. Nakamura, and N. Henderson, 2014a: Causes and predictability of the 2011–14 California drought. NOAA Drought Task Force Rep., 40 pp., https://doi.org/10.7289/V58K771F.

——, and Coauthors, 2014b: Dynamical and thermodynamical causes of large-scale changes in the hydrological cycle over North America in response to global warming. *J. Climate*, **27**, 7921–7948, https://doi.org/10.1175/JCLI-D-14-00153.1.

——, M. Hoerling, S. Schubert, H. Wang, B. Lyon, A. Kumar, J. Nakamura, and N. Henderson, 2015: Causes of the 2011–14 California drought. *J. Climate*, **28**, 6997–7024, https://doi.org/10.1175/JCLI-D-14-00860.1.

Semenov, V. A., T. Martin, L. K. Behrens, and M. Latif, 2015: Arctic sea ice area in CMIP3 and CMIP5 climate model ensembles—Variability and change. *Cryosphere Discuss.*, **9**, 1077–1131, https://doi.org/10.5194/tcd-9-1077-2015.

Shepherd, T. G., 2015: Climate science: The dynamics of temperature extremes. *Nature*, **522**, 425–427, https://doi.org/10.1038/522425a.

Simpson, I. R., T. A. Shaw, and R. Seager, 2014: A diagnosis of the seasonally and longitudinally varying midlatitude circulation response to global warming. *J. Atmos. Sci.*, **71**, 2489–2515, https://doi.org/10.1175/JAS-D-13-0325.1.

——, R. Seager, M. Ting, and T. A. Shaw, 2016: Causes of change in Northern Hemisphere winter meridional wind and regional hydroclimate. *Nat. Climate Change*, **6**, 65–70, https://doi.org/10.1038/NCLIMATE2783.

Stott, P. A., and Coauthors, 2016: Attribution of extreme weather and climate-related events. *Wiley Interdiscip. Rev.: Climate Change*, **7**, 23–41, https://doi.org/10.1002/wcc.380.

Swain, D. L., M. Tsiang, M. Haugen, D. Singh, A. Charland, B. Rajaratnam, and N. S. Diffenbaugh, 2014: The extraordinary California drought of 2013/14: Character, context and the role of climate change [in "Explaining Extreme Events of 2013 from a Climate Perspective"]. *Bull. Amer. Meteor. Soc.*, **95** (9), S3–S7.

Teng, H., and G. Branstator, 2017: Causes of extreme ridges that induce California droughts. *J. Climate*, **30**, 1477–1492, https://doi.org/10.1175/JCLI-D-16-0524.1.

Uppala, S. M., and Coauthors, 2005: The ERA-40 Re-Analysis. *Quart. J. Roy. Meteor. Soc.*, **131**, 2961–3012, https://doi.org/10.1256/qj.04.176.

Wang, S.-Y., L. Hipps, R. R. Gillies, and J.-H. Yoon, 2014: Probable causes of the abnormal ridge accompanying the 2013–2014 California drought: ENSO precursor and anthropogenic warming footprint. *Geophys. Res. Lett.*, **41**, 3220–3226, https://doi.org/10.1002/2014GL059748.

Watson, P. A. G., A. Weisheimer, J. R. Knight, and T. N. Palmer, 2016: The role of the tropical West Pacific in the extreme Northern Hemisphere winter of 2013/14. *J. Geophys. Res. Atmos.*, **121**, 1698–1714, https://doi.org/10.1002/2015JD024048.

Williams, A. P., R. Seager, J. T. Abatzoglou, B. I. Cook, J. E. Smerdon, and E. R. Cook, 2015: Contribution of anthropogenic warming to California drought during 2012–2014. *Geophys. Res. Lett.*, **42**, 6819–6828, https://doi.org/10.1002/2015GL064924.